JACS
JOURNAL OF THE AMERICAN CHEMICAL SOCIETY
pubs.acs.org/JACS
Communication

Unraveling a Stable 16-Ring Aluminophosphate DNL-11 through Three-Dimensional Electron Diffraction for Atmospheric Water Harvesting

Chenyang Nie, Nana Yan, Chenyi Liao, Chao Ma, Xiaona Liu, Jing Wang, Guohui Li, Peng Guo,* and Zhongmin Liu*

Cite This: J. Am. Chem. Soc. 2024, 146, 10257−10262
Read Online
ACCESS | Metrics & More | Article Recommendations | Supporting Information

ABSTRACT: Sorption-based atmospheric water harvesting (AWH) is a promising solution for addressing water scarcity. Developing cost-effective and stable water adsorbents with high water uptake capacity and a low-temperature regeneration requirement is a crucially important procedure. In this Communication, we present a novel and stable aluminophosphate (AlPO) molecular sieve (MS) named DNL-11 with 16-ring channels synthesized by using an affordable and commercialized organic structure directing agent (OSDA), whose crystallographic structure is elucidated by three-dimensional electron diffraction (3D ED). DNL-11 exhibits a significant water uptake capacity (189 mg/g) at a very low vapor pressure (5% relative humidity at 30 °C). In addition, most of the adsorbed water can be effortlessly removed by purging N_2 at 25 °C under ambient pressure conditions. This may expand the possibility of AWH under extreme drought conditions.

Water is fundamental to life's existence, yet people facing water scarcity are increasingly imperiled due to exponential population growth. Currently, around 2 billion individuals worldwide lack access to safe drinking water, while approximately 3.6 billion people are suffering from adequate sanitation facilities.[1] Seawater desalination offers a viable solution for water scarcity; however, it is energy-intensive and less practical for landlocked countries with limited access to seawater.[2,3] Moreover, the atmosphere, considered a natural water storage warehouse, allows for extraction of water through three primary methods: fog collection, dew collection or refrigeration, and sorption-based atmospheric water harvesting (AWH).[4−7] Fog collection is geographically limited, while dew collection or refrigeration requires substantial energy consumption.[8−10] Sorption-based AWH provides a promising solution for the treatment of arid areas. This technology captures atmospheric water vapor by utilizing sorbents, releases it with low-grade energy sources such as solar or waste heat, and then condenses the vapor to produce potable water.[11] Consequently, a potentially superior water sorbent should at least exhibit the following characteristics: 1) inherently pronounced water uptake capacity, 2) consistent water retention ability through successive cycles, and 3) low temperature requirements for regeneration.[12,13]

The fascinating and functional crystalline porous materials such as metal−organic frameworks (MOFs) and covalent organic frameworks (COFs) are utilized for water harvesting, especially in the MOF research field.[14−19] For example, MOF-801 can harvest 2.8 L of water per kilogram daily even at a relative humidity (RH) of 20%.[20] Following these advancements, zeolites, featuring interconnected TO_4 tetrahedra (T = Al and Si) with well-defined cavities or channels, are also emerging as a noteworthy option due to their low-cost, ease of fabrication, and high thermal stability. For example, low-silica **FAU**- and **LTA**-type zeolites display high water uptakes and multiple water adsorption cycles,[21] however, the regeneration of zeolites often requires elevated temperatures, occasionally combining with high vacuum conditions. This is attributed to the strong interactions between water molecules and the inorganic cations embedded in the negative zeolite framework.[22] Subsequently, cage-based AlPO MSs with a neutral framework (free of cations) and small-pore openings such as those of the **LTA**- and **CHA**-types, exhibit outstanding water adsorption capabilities.[23−26] However, moderately high-temperature conditions during regeneration are still needed. Consequently, AlPO MSs with high water adsorption capacity, robust stability, and easy regeneration are highly sought after in the field of AWH.

During the AWH process, structural characterization at the atomic level is crucially important for understanding the structure−activity relationship. Traditional X-ray crystallography, including single-crystal (SCXRD) and powder X-ray diffraction (PXRD), is widely used for structure determination, from initial structure solution to the following structural refinement. SCXRD, a well-established method, necessitates crystals over 20 μm for in-house analysis. Although PXRD is suitable for structural characterizations of nanocrystals, it still faces challenges such as peak overlap, impurities, and a

Received: January 29, 2024
Revised: April 3, 2024
Accepted: April 3, 2024
Published: April 5, 2024

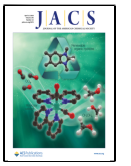

https://doi.org/10.1021/jacs.4c01393
J. Am. Chem. Soc. 2024, 146, 10257−10262

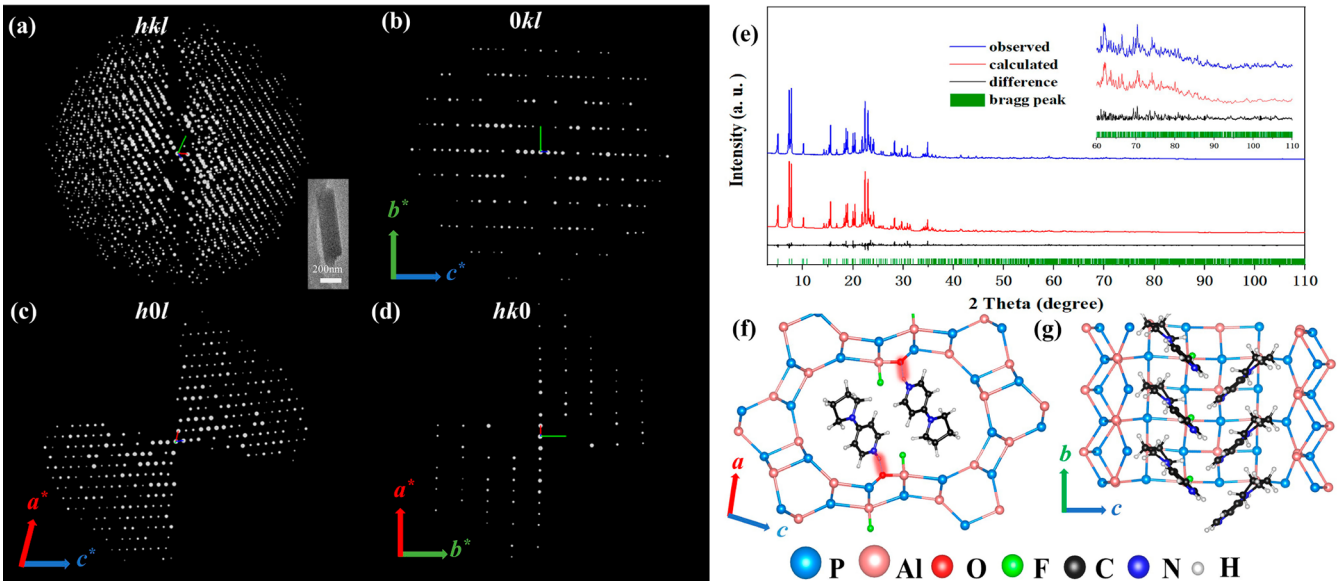

Figure 1. (a) 3D reciprocal lattice of DNL-11-as. (b–d) Reciprocal planes perpendicular to a^*, b^*, and c^*, respectively. (e) Rietveld refinement plots for DNL-11-as (λ = 1.5406 Å). (f) The 16-ring channel of DNL-11-as along the [010] direction, the red area represents the interaction between protonated OSDAs and framework oxygens. (g) The OSDAs arrangement of DNL-11-as.

complicated initial structure solution. Nonetheless, PXRD is beneficial for structural refinement, particularly in studying host–guest interactions in crystalline porous materials.[27,28] Recently, three-dimensional electron diffraction (3D ED) has emerged as a significant breakthrough in the electron crystallography.[29−38] It has displayed its efficacy in determining the crystallographic structures of unknown nanocrystals including unit cell parameters, space groups, and atomic coordinates. In recent decades, more than 30 novel zeolites have been successfully determined by 3D ED.[39−42] The recently developed continuous rotation electron diffraction (cRED) can collect ED data in a short time with a continuous way, which not only greatly reduces radiation damage during the data collection, but also significantly improves the data quality.[43,44] Therefore, cRED is instrumental in unraveling the complexities of nanoscale crystalline functional materials.[45]

In this study, we utilized commercialized 4-pyrrolidinopyridine as an OSDA to synthesize a novel AlPO MS denoted as DNL-11. The initial structural model of DNL-11 was solved by using the cRED technique, and the positions of OSDAs were identified through a combination of PXRD refinement and the simulated annealing (SA) algorithm. It turns out DNL-11 has a one-dimensional (1D) 16-ring straight channel, and OSDAs performed supramolecular assembly by $\pi-\pi$ interaction in the channels. Additionally, DNL-11 demonstrated a water adsorption capacity of 189 mg/g at a remarkably low pressure of P/P_0 = 0.05 and 30 °C. Notably, its adsorption capacity remained largely consistent after 10 cycles. More interestingly, the majority of the adsorbed water (82%) can be removed by purging N_2 at 25 °C under ambient pressure conditions. DNL-11 is crucial for broadening the application scope of AWH technology in extremely arid regions.

DNL-11 was obtained by the hydrothermal synthesis using the commercialized 4-pyrrolidinopyridine as the OSDA (Figure S1). By optimizing the chemical gel compositions, DNL-11 was finally crystallized at the gel with the molar composition of 1.0 P_2O_5:1.0 Al_2O_3:3.0 OSDA:30 TEG:40 H_2O (Tables S1 and S2). The SEM image shows that the as-made DNL-11 (denoted as DNL-11-as) possesses nanorod morphology, which hinders its structural elucidation by conventional SCXRD (Figure S2). Therefore, we utilized the cRED technique to unravel the crystallographic structure of DNL-11-as. A high quality of cRED data set of DNL-11-as was collected within 3 min. The reconstructed 3D reciprocal lattices of DNL-11-as were depicted in Figure 1a. The monoclinic unit cell parameters could be deduced from this data set, and possible space groups ($P2_1$ and $P2_1/m$) could be obtained based on the reflection conditions as demonstrated in Figure 1b–d. The intensity for each *hkl* indices was extracted by utilizing XDS software.[46] Its initial structural model was solved by the direct method implemented in SHELXT with the space group of $P2_1$. There are 8 T atoms, 16 O atoms, and 1 F^- ion identified in the asymmetric unit (Table S3–S4).

In the framework of DNL-11-as, a 1D 16-ring channel along the *b*-axis can be observed. It is noteworthy that the Al1 atom exposed to the channel coordinates with 4 O atoms and 1 F^- ion, resulting in the formation of a penta-coordinated aluminum. This result aligns with the observations from ^{27}Al NMR and ^{19}F NMR spectroscopy (Figures S3 and S4). Although electron densities within DNL-11-as channels could be identified, it is still challenging to finalize based solely on the 3D ED data. Therefore, DNL-11-as was finalized by Rietveld refinement against PXRD combined with SA algorithm (Figure 1e and Table S5). It is crucially important to point out there are two columns of OSDAs along the *b*-axis within the 1D 16-ring channel. All 4-pyrrolidinepyridines are protonated (Figure S5) and interacted with the framework oxygens via hydrogen bonding (Figure 1f). Meanwhile, as shown in Figures 1g, the arrangement of OSDAs running along the *b*-axis indicates that there are $\pi-\pi$ interactions between them.

DNL-11-as underwent calcination at 800 °C to remove the OSDAs and F^- ions, resulting in the calcined form termed DNL-11-cal (Figure S6). DNL-11-cal maintains the good crystallinity verified by PXRD data and BET (Figures S7 and S8). The crystallographic structure of DNL-11-cal was also determined by combining cRED with the PXRD technique

https://doi.org/10.1021/jacs.4c01393
J. Am. Chem. Soc. 2024, 146, 10257−10262

(Tables S6 and S7 and Figures S9 and S10). From a structural point of view, the structure of DNL-11-cal is highly related to AlPO-36 (**ATS**). The building layer in the *ac* plane of DNL-11-cal is the same as that of AlPO-36 (designated as the *ats* layer). As shown in Figure 2, AlPO-36 can be considered as *ats*

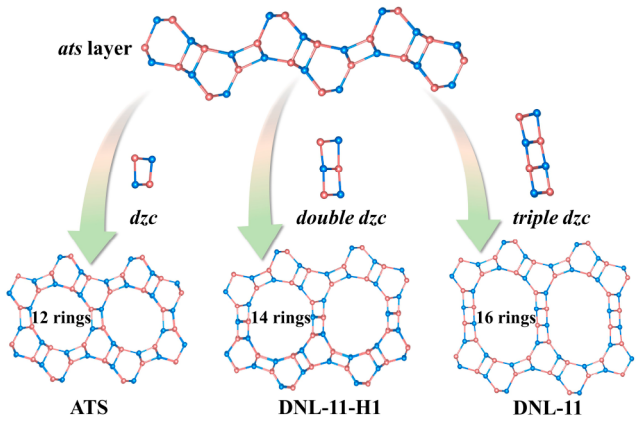

Figure 2. Building scheme of **ATS**, DNL-11-H1, and DNL-11. Three structures share identical *ats* layers but are pillared by three distinct types of chains. Oxygen atoms have been omitted for the sake of clarity.

building layers interconnected by *dzc* chains, which can be described as edge-shared single 4-rings (*s4rs*) (Figure S11). It is of interest to note that in the DNL-11-cal, *ats* layers are supported by unprecedented chains termed triple *dzc* chains (Figure 2 and Figure S12). In this case, a hypothetical AlPO structure named DNL-11-H1 with a 1D 14-ring channel system will be built, in which the unique double *dzc* chains can be identified.

As previously mentioned, AlPO MSs have found widespread application in water adsorption. To establish a performance benchmark, we conducted water adsorption tests on AlPO-42 (**LTA**), AlPO-34 (**CHA**), AlPO-17 (**ERI**), AlPO-5 (**AFI**), AlPO-11 (**AEL**), and DNL-11 under the isothermal condition of 30 °C as shown in Figure 3a and Figure S13. On the one hand, cage-based AlPO structures, exemplified by AlPO-34, AlPO-42, and AlPO-17, exhibit notable water adsorption capacities. These structures show pressure-induced S-shaped steep adsorption isotherms, which mainly occur between the pressure ranges of P/P_0 = 0.05 and P/P_0 = 0.15. On the other hand, channel-based AlPOs like AlPO-5 and AlPO-11, characterized by their one-dimensional channel structures, tend to exhibit a more limited adsorption capacity. Although DNL-11 features a channel-based architecture, its water adsorption capacity at 30 °C is approximately 380 mg/g at a pressure of P/P_0 = 0.96. This performance is comparable to that of the cage-based AlPO-34 and is only slightly surpassed by AlPO-42. It is worth noting that the water adsorption capacity of DNL-11 rises rapidly in the range of P/P_0 = 0−0.05, reaching an adsorption capacity of 189 mg/g (Figure 3b and Figure S14). In an assessment of water adsorption recyclability under a pressure of P/P_0 = 0.05, DNL-11 demonstrates a consistent adsorption capacity with negligible variation over the span of more than 10 cycles (Figure 3c). It indicates DNL-11 is a highly potential adsorptive material for water harvesting, particularly effective in arid or extremely arid regions. 82% of water in the hydrated DNL-11 can be efficiently removed by purging with N_2 at 25 °C under ambient

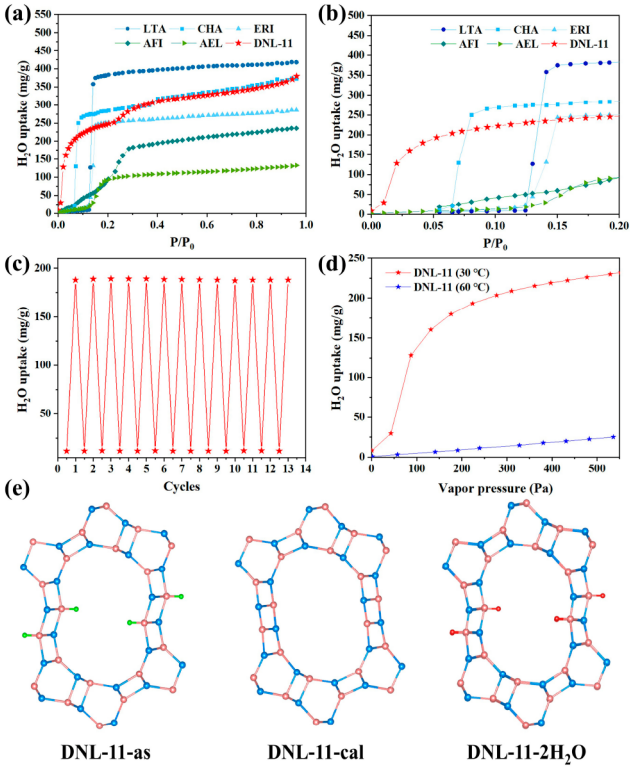

Figure 3. (a) Adsorption isotherms of DNL-11, AlPO-34 (**CHA**), AlPO-42 (**LTA**), AlPO-17 (**ERI**), AlPO-5 (**AFI**), and AlPO-11 (**AEL**) at 30 °C. (b) The enlarged view of the part of (a). (c) Cyclic water adsorption curve of DNL-11 at 30 °C and P/P_0 = 0.05. (d) Adsorption isotherms of DNL-11 at 30 and 60 °C, respectively. (e) Projections of DNL-11-as, DNL-11-cal and DNL-11-2H_2O along the *b* axis (OSDAs in the DNL-11-as are omitted for clarity).

pressure conditions. The remaining water molecules are completely desorbed in the subsequent heating process (Figure S15). Fully hydrated DNL-11, saturated at 96% RH and 30 °C, can be completely dehydrated at 60 °C within 85 min (Figure S16). Water adsorption isotherms of DNL-11 at 30 and 60 °C were also investigated (Figure 3d). It turns out that the water adsorption of DNL-11 decreases rapidly with a temperature increase of 30 °C. It indicates that, at the specific working pressure of 210 Pa, DNL-11 can collect 180 mg/g of water through the temperature fluctuation between 30 and 60 °C. Its exceptional performance under ultralow humidity conditions, particularly at 5% RH and 30 °C, highlights its potential for expanding the application scope in AWH.

To successfully utilize DNL-11 as an adsorbent in the AWH system, it is essential to comprehend its mechanism of water adsorption, particularly the locations of adsorbed water that have strong interactions with the framework. Therefore, we utilized a mechanical pump combined with a molecular pump to remove most of the adsorbed water from the hydrated DNL-11. The desorption data as illustrated in Figure S17 shows that approximately two water molecules per-channel are adsorbed in the DNL-11 (denoted as DNL-11-2H_2O). The PXRD data of DNL-11-2H_2O was collected (Table S8−S9 and Figure S18), and final refinement results show that two water molecules coordinate with Al1 and Al5, resulting in the penta-coordinated aluminum. Such results are consistent with the theoretical calculations (Table S10). Interestingly, the adsorption locations of water molecules in DNL-11-2H_2O

https://doi.org/10.1021/jacs.4c01393
J. Am. Chem. Soc. 2024, 146, 10257−10262

are similar to the positions of F^- ions in DNL-11-as (Figure 3e). Since DNL-11-cal possesses a 1D 16-ring superlarge pore structure with open aluminum sites facing the pores, water molecules can easily penetrate these pores under extremely low pressure and then coordinate with open aluminum sites. The *ab initio* molecular dynamics (MD) simulations indicate that successive water molecules form clusters via hydrogen bonding with coordinating water (Figure S19). Initially, these clusters do not align with the DNL-11 channels, preventing the pore filling process until water pressure facilitates the creation of water bridges across the channels connecting the water clusters. Consequently, this progression delays the adsorption isotherm of DNL-11, resulting in the formation of a hysteresis loop (Figure S13).[47]

In summary, a new and stable AlPO MS DNL-11 was successfully synthesized using cost-effective and commercially available OSDA and its crystallographic structure was elucidated by the cRED technique. DNL-11 features unique 1D 16-ring channels with unprecedented triple *dzc*. It exhibits remarkable water adsorption capacity at 5% RH and 30 °C, which is meaningful for atmospheric water collection under drought conditions. The primary mechanism behind water adsorption in DNL-11 at low RH values is attributed to the presence of accessible open Al sites. A potential synthetic strategy to enhance this property could involve the introduction of F^- ions coordinated with the framework, which would aid in creating more open Al sites.

■ ASSOCIATED CONTENT

Supporting Information

The Supporting Information is available free of charge at https://pubs.acs.org/doi/10.1021/jacs.4c01393.

Synthesis, characterization, theoretical calculation, and crystallographic data (PDF)

Accession Codes

CCDC 2311458 and 2322522 contain the supplementary crystallographic data for this paper. These data can be obtained free of charge via www.ccdc.cam.ac.uk/data_request/cif, or by emailing data_request@ccdc.cam.ac.uk, or by contacting The Cambridge Crystallographic Data Centre, 12 Union Road, Cambridge CB2 1EZ, UK; fax: +44 1223 336033.

■ AUTHOR INFORMATION

Corresponding Authors

Zhongmin Liu − *National Engineering Research Center of Lower-Carbon Catalysis Technology, Dalian Institute of Chemical Physics, Chinese Academy of Sciences, Dalian 116023 Liaoning, China; University of Chinese Academy of Sciences, Beijing 100049, China*; Email: zml@dicp.ac.cn

Peng Guo − *National Engineering Research Center of Lower-Carbon Catalysis Technology, Dalian Institute of Chemical Physics, Chinese Academy of Sciences, Dalian 116023 Liaoning, China; University of Chinese Academy of Sciences, Beijing 100049, China;* orcid.org/0000-0001-5392-3915; Email: pguo@dicp.ac.cn

Authors

Chenyang Nie − *National Engineering Research Center of Lower-Carbon Catalysis Technology, Dalian Institute of Chemical Physics, Chinese Academy of Sciences, Dalian 116023 Liaoning, China; University of Chinese Academy of Sciences, Beijing 100049, China*

Nana Yan − *National Engineering Research Center of Lower-Carbon Catalysis Technology, Dalian Institute of Chemical Physics, Chinese Academy of Sciences, Dalian 116023 Liaoning, China*

Chenyi Liao − *Laboratory of Molecular Modeling and Design, State Key Laboratory of Molecular Reaction Dynamics, Dalian Institute of Chemical Physics, Chinese Academy of Sciences, Dalian 116023 Liaoning, China;* orcid.org/0000-0002-1681-205X

Chao Ma − *National Engineering Research Center of Lower-Carbon Catalysis Technology, Dalian Institute of Chemical Physics, Chinese Academy of Sciences, Dalian 116023 Liaoning, China; University of Chinese Academy of Sciences, Beijing 100049, China; School of Chemistry, Dalian University of Technology, Dalian 116024 Liaoning, China*

Xiaona Liu − *National Engineering Research Center of Lower-Carbon Catalysis Technology, Dalian Institute of Chemical Physics, Chinese Academy of Sciences, Dalian 116023 Liaoning, China*

Jing Wang − *National Engineering Research Center of Lower-Carbon Catalysis Technology, Dalian Institute of Chemical Physics, Chinese Academy of Sciences, Dalian 116023 Liaoning, China;* orcid.org/0000-0002-4185-0373

Guohui Li − *Laboratory of Molecular Modeling and Design, State Key Laboratory of Molecular Reaction Dynamics, Dalian Institute of Chemical Physics, Chinese Academy of Sciences, Dalian 116023 Liaoning, China;* orcid.org/0000-0001-8223-705X

Complete contact information is available at: https://pubs.acs.org/10.1021/jacs.4c01393

Author Contributions

The manuscript was written through contributions of all authors. All authors have given approval to the final version of the manuscript.

Notes

The authors declare no competing financial interest.

■ ACKNOWLEDGMENTS

This work is supported by the National Natural Science Foundation of China (Nos. 22288101, 21972136, 21991090, 21991091, 22372156, 22302195, and 22102177). We sincerely thank Zhaojin Yang, Xiaoge Jiao, and Jiashuo Zhang from Beishide Instrument Technology (Beijing) Co., Ltd. for their assistance with the BSD-DVS instrument and data processing in the thermal desorption experiment.

■ REFERENCES

(1) United Nations. *The United Nations World Water Development Report 2023: Partnerships and Cooperation for Water*; UNESCO, 2023.
(2) Elimelech, M.; Phillip, W. A. The Future of Seawater Desalination: Energy, Technology, and the Environment. *Science.* **2011**, *333*, 712−717.
(3) Kocher, J. D.; Menon, A. K. Addressing Global Water Stress Using Desalination and Atmospheric Water Harvesting: A Thermodynamic and Technoeconomic Perspective. *Energy Environ. Sci.* **2023**, *16*, 4983−4993.
(4) Lord, J.; Thomas, A.; Treat, N.; Forkin, M.; Bain, R.; Dulac, P.; Behroozi, C. H.; Mamutov, T.; Fongheiser, J.; Kobilansky, N.; Washburn, S.; Truesdell, C.; Lee, C.; Schmaelzle, P. H. Global Potential for Harvesting Drinking Water from Air Using Solar Energy. *Nature.* **2021**, *598*, 611−617.

(5) Gido, B.; Friedler, E.; Broday, D. M. Assessment of Atmospheric Moisture Harvesting by Direct Cooling. *Atmos. Res.* **2016**, *182*, 156−162.
(6) Gu, G.; Gu, G.; Wang, J.; Yao, X.; Ju, J.; Cheng, G.; Du, Z. A Water Collection System with Ultra-High Harvest Rate and Ultra-Low Energy Consumption by Integrating Triboelectric Plasma. *Nano Energy.* **2022**, *96*, 107081.
(7) Lu, H.; Shi, W.; Guo, Y.; Guan, W.; Lei, C.; Yu, G. Materials Engineering for Atmospheric Water Harvesting: Progress and Perspectives. *Adv. Mater.* **2022**, *34*, No. e2110079.
(8) Kennedy, B. S.; Boreyko, J. B. Bio-Inspired Fog Harvesting Meshes: A Review. *Adv. Funct. Mater.* **2023**, 20230616.
(9) Bagheri, F. Performance Investigation of Atmospheric Water Harvesting Systems. *Water Resour. Ind.* **2018**, *20*, 23−28.
(10) Shi, W.; Guan, W.; Lei, C.; Yu, G. Sorbents for Atmospheric Water Harvesting: From Design Principles to Applications. *Angew. Chem., Int. Ed.* **2022**, *61*, No. e202211267.
(11) Entezari, A.; Esan, O. C.; Yan, X.; Wang, R.; An, L. Sorption-Based Atmospheric Water Harvesting: Materials, Components, Systems, and Applications. *Adv. Mater.* **2023**, *35*, 2210957.
(12) Kalmutzki, M. J.; Diercks, C. S.; Yaghi, O. M. Metal−Organic Frameworks for Water Harvesting from Air. *Adv. Mater.* **2018**, *30*, 1704304.
(13) Hanikel, N.; Prévot, M. S.; Yaghi, O. M. MOF Water Harvesters. *Nat. Nanotechnol.* **2020**, *15*, 348−355.
(14) Nguyen, H. L.; Gropp, C.; Hanikel, N.; Möckel, A.; Lund, A.; Yaghi, O. M. Hydrazine-Hydrazide-Linked Covalent Organic Frameworks for Water Harvesting. *ACS Cent. Sci.* **2022**, *8*, 926−932.
(15) Chen, L. H.; Han, W. K.; Yan, X.; Zhang, J.; Jiang, Y.; Gu, Z. G. A Highly Stable Ortho-Ketoenamine Covalent Organic Framework with Balanced Hydrophilic and Hydrophobic Sites for Atmospheric Water Harvesting. *ChemSusChem* **2022**, *15*, No. e202201824.
(16) Alezi, D.; Oppenheim, J. J.; Sarver, P. J.; Iliescu, A.; Dinakar, B.; Dincă, M. Tunable Low−Relative Humidity and High−Capacity Water Adsorption in a Bibenzotriazole Metal−Organic Framework. *J. Am. Chem. Soc.* **2023**, *145*, 25233−25241.
(17) Lu, F.-F.; Gu, X.-W.; Wu, E.; Li, B.; Qian, G. Systematic Evaluation of Water Adsorption in Isoreticular Uio-Type Metal−Organic Frameworks. *J. Mater. Chem. A* **2023**, *11*, 1246−1255.
(18) Zhu, N. X.; Wei, Z. W.; Chen, C. X.; Xiong, X. H.; Xiong, Y. Y.; Zeng, Z.; Wang, W.; Jiang, J. J.; Fan, Y. N.; Su, C. Y. High Water Adsorption MOFs with Optimized Pore-Nanospaces for Autonomous Indoor Humidity Control and Pollutants Removal. *Angew. Chem., Int. Ed.* **2022**, *61*, No. e202112097.
(19) Zheng, J.; Vemuri, R. S.; Estevez, L.; Koech, P. K.; Varga, T.; Camaioni, D. M.; Blake, T. A.; McGrail, B. P.; Motkuri, R. K. Pore-Engineered Metal-Organic Frameworks with Excellent Adsorption of Water and Fluorocarbon Refrigerant for Cooling Applications. *J. Am. Chem. Soc.* **2017**, *139*, 10601−10604.
(20) Kim, H.; Yang, S.; Rao, S. R.; Narayanan, S.; Kapustin, E. A.; Furukawa, H.; Umans, A. S.; Yaghi, O. M.; Wang, E. N. Water Harvesting from Air with Metal-Organic Frameworks Powered by Natural Sunlight. *Science.* **2017**, *356*, 430−434.
(21) Kim, K.-M.; Oh, H.-T.; Lim, S.-J.; Ho, K.; Park, Y.; Lee, C.-H. Adsorption Equilibria of Water Vapor on Zeolite 3A, Zeolite 13X, and Dealuminated Y Zeolite. *J. Chem. Eng. Data* **2016**, *61*, 1547−1554.
(22) Gabruś, E.; Nastaj, J.; Tabero, P.; Aleksandrzak, T. Experimental Studies on 3A and 4A Zeolite Molecular Sieves Regeneration in Tsa Process: Aliphatic Alcohols Dewatering−Water Desorption. *Chem. Eng. J.* **2015**, *259*, 232−242.
(23) Abd Elwadood, S. N.; Dumée, L. F.; Al Wahedi, Y.; Al Alili, A.; Karanikolos, G. N. Aluminophosphate - Based Adsorbents for Atmospheric Water Generation. *J. Water Process.* **2022**, *49*, 103099.
(24) Krajnc, A.; Varlec, J.; Mazaj, M.; Ristić, A.; Logar, N. Z.; Mali, G. Superior Performance of Microporous Aluminophosphate with LTA Topology in Solar-Energy Storage and Heat Reallocation. *Adv. Energy Mater.* **2017**, *7*, 1601815.
(25) Yuhas, B. D.; Wilson, K.; Miller, M. A.; Sinkler, W.; Yu, H.; Mowat, J. P. S. Alpo-91: A 16-Layer Abc-6 Aluminophosphate with Five Distinct Cage Types. *ACS Materials Lett.* **2021**, *3*, 1752−1756.
(26) Shi, J.; Hu, J.; Wu, Q.; Chen, W.; Dong, Z.; Zheng, A.; Ma, Y.; Meng, X.; Xiao, F.-S. A Six-Membered Ring Molecular Sieve Achieved by a Reconstruction Route. *J. Am. Chem. Soc.* **2023**, *145*, 7712−7717.
(27) Chu, W.; Liu, X.; Yang, Z.; Nakata, H.; Tan, X.; Liu, X.; Xu, L.; Guo, P.; Li, X.; Zhu, X. Constrained Al Sites in FER-Type Zeolites. *Chin. J. Catal.* **2021**, *42*, 2078−2087.
(28) Yan, N.; Wang, L.; Liu, X.; Wu, P.; Sun, T.; Xu, S.; Han, J.; Guo, P.; Tian, P.; Liu, Z. A Novel Approach for Facilitating the Targeted Synthesis of Silicoaluminophosphates. *J. Mater. Chem. A* **2018**, *6*, 24186−24193.
(29) Kolb, U.; Gorelik, T.; Kübel, C.; Otten, M. T.; Hubert, D. Towards Automated Diffraction Tomography: Part I—Data Acquisition. *Ultramicroscopy.* **2007**, *107*, 507−513.
(30) Kolb, U.; Gorelik, T.; Otten, M. T. Towards Automated Diffraction Tomography. Part II–Cell Parameter Determination. *Ultramicroscopy* **2008**, *108*, 763−772.
(31) Kolb, U.; Krysiak, Y.; Plana-Ruiz, S. Automated Electron Diffraction Tomography - Development and Applications. *Acta Crystallogr.* **2019**, *B75*, 463−474.
(32) Wan, W.; Sun, J.; Su, J.; Hovmoller, S.; Zou, X. Three-Dimensional Rotation Electron Diffraction: Software Red for Automated Data Collection and Data Processing. *J. Appl. Crystallogr.* **2013**, *46*, 1863−1873.
(33) Smeets, S.; Zou, X.; Wan, W. Serial Electron Crystallography for Structure Determination and Phase Analysis of Nanocrystalline Materials. *J. Appl. Crystallogr.* **2018**, *51*, 1262−1273.
(34) Nannenga, B. L.; Shi, D.; Leslie, A. G. W.; Gonen, T. High-Resolution Structure Determination by Continuous-Rotation Data Collection in Microed. *Nat. Methods.* **2014**, *11*, 927−930.
(35) Shi, D.; Nannenga, B. L.; Iadanza, M. G.; Gonen, T. Three-Dimensional Electron Crystallography of Protein Microcrystals. *eLife* **2013**, *2*, No. e01345.
(36) Palatinus, L.; Correa, C. A.; Steciuk, G.; Jacob, D.; Roussel, P.; Boullay, P.; Klementova, M.; Gemmi, M.; Kopecek, J.; Domeneghetti, M. C.; Camara, F.; Petricek, V. Structure Refinement Using Precession Electron Diffraction Tomography and Dynamical Diffraction: Tests on Experimental Data. *Acta Crystallogr.* **2015**, *71*, 740−751.
(37) Zhang, D.; Oleynikov, P.; Hovmöller, S.; Zou, X. Collecting 3D Electron Fiffraction Data by the Rotation Method. *Z. Kristallogr.* **2010**, *225*, 94−102.
(38) Gemmi, M.; Oleynikov, P. Scanning Reciprocal Space for Solving Unknown Structures: Energy Filtered Diffraction Tomography and Rotation Diffraction Tomography Methods. *Z. Kristallogr.* **2013**, *228*, 51−58.
(39) Li, J.; Gao, Z. R.; Lin, Q.-F.; Liu, C.; Gao, F.; Lin, C.; Zhang, S.; Deng, H.; Mayoral, A.; Fan, W.; Luo, S.; Chen, X.; He, H.; Camblor, M. A.; Chen, F.-J.; Yu, J. A 3D Extra-Large-Pore Zeolite Enabled by 1D-to-3D Topotactic Condensation of a Chain Silicate. *Science.* **2023**, *379*, 283−287.
(40) Lin, Q.-F.; Gao, Z. R.; Lin, C.; Zhang, S.; Chen, J.; Li, Z.; Liu, X.; Fan, W.; Li, J.; Chen, X.; Camblor, M. A.; Chen, F.-J. A Stable Aluminosilicate Zeolite with Intersecting Three-Dimensional Extra-Large Pores. *Science.* **2021**, *374*, 1605−1608.
(41) Liu, X.; Liu, L.; Pan, T.; Yan, N.; Dong, X.; Li, Y.; Chen, L.; Tian, P.; Han, Y.; Guo, P.; Liu, Z. The Complex Crystal Structure and Abundant Local Defects of Zeolite EMM-17 Unraveled by Combined Electron Crystallography and Microscopy. *Angew. Chem. Int. Ed.* **2021**, *60*, 24227−24233.
(42) Ma, C.; Liu, X.; Nie, C.; Chen, L.; Tian, P.; Xu, H.; Guo, P.; Liu, Z. Applications of X-Ray and Electron Crystallography in Structural Investigations of Zeolites. *Chem. J. Chin. Univ.* **2021**, *42*, 188−200.
(43) Wang, Y.; Takki, S.; Cheung, O.; Xu, H.; Wan, W.; Öhrström, L.; Inge, A. K. Elucidation of the Elusive Structure and Formula of the

https://doi.org/10.1021/jacs.4c01393
J. Am. Chem. Soc. 2024, 146, 10257−10262

Active Pharmaceutical Ingredient Bismuth Subgallate by Continuous Rotation Electron Diffraction. *Chem. Commun.* **2017**, *53*, 7018−7021.
(44) Wang, J.; Ma, C.; Liu, J.; Liu, Y.; Xu, X.; Xie, M.; Wang, H.; Wang, L.; Guo, P.; Liu, Z. Pure Silica with Ordered Silanols for Propylene/Propane Adsorptive Separation Unraveled by Three-Dimensional Electron Diffraction. *J. Am. Chem. Soc.* **2023**, *145*, 6853−6860.
(45) Huang, Z.; Willhammar, T.; Zou, X. Three-Dimensional Electron Diffraction for Porous Crystalline Materials: Structural Determination and Beyond. *Chem. Sci.* **2021**, *12*, 1206−1219.
(46) Kabsch, W. XDS. *Acta Crystallogr., Sect. D: Biol. Crystallogr.* **2010**, *66*, 125−132.
(47) Liu, L.; Tan, S.; Horikawa, T.; Do, D. D.; Nicholson, D.; Liu, J. Water Adsorption on Carbon - a Review. *Adv. Colloid Interface Sci.* **2017**, *250*, 64−78.

https://doi.org/10.1021/jacs.4c01393
J. Am. Chem. Soc. 2024, 146, 10257−10262